PCCP

PAPER

Cite this: DOI: 10.1039/c8cp02547a

Reconstructing stochastic attractors from nanoscale experiments on a non-equilibrium reaction

Cédric Barroo, *[ab] Valérie Voorsluijs, [bc] Thierry Visart de Bocarmé, [ab] Pierre Gaspard[b] and Yannick De Decker[bc]

Received 21st April 2018,
Accepted 2nd August 2018

DOI: 10.1039/c8cp02547a

rsc.li/pccp

We studied the catalytic $NO_2(g) + H_2(g)/Pt$ system on model platinum catalysts with nanoscale spatial resolution by means of field emission microscopy (FEM). While the surface of the catalyst is in a non-reactive state at low H_2 partial pressure, bursts of activity are observed when increasing this parameter. These kinetic instabilities subsequently evolve towards self-sustained periodic oscillations for a wide range of pressures. Combining time series analyses and numerical simulations of a simple reaction model, we clarify how these observations fit in the traditional classification of dynamical systems. In particular, reconstructions of the probability density around oscillating trajectories show that the experimental system defines a crater-like structure in probability space. The experimental observations thus correspond to a noise-perturbed limit cycle emerging from a nanometric reactive system. This conclusion is further supported by comparison with stochastic simulations of the proposed chemical model. The obtained results and simulations pave the way towards a better understanding of reactive nanosystems.

I Introduction

Field emission microscopy (FEM) is a powerful method to study the dynamics of solid–gas interactions taking place on the surface of a nanosized metal tip, the extremity of which acts as a model catalyst.[1–4] FEM is based on the emission of electrons from the sample in the presence of an electric field. According to the Fowler–Nordheim equation,[5,6] for a constant electrical field and temperature, the current density emitted from a metal sample depends only on its local work function. The work function depends on the crystallographic orientation of the facets of the metallic sample and may also change in the presence of adsorbates or surface reconstructions.[7–9] Consequently, the adsorbate-induced local variations of work function translate on the screen of the microscope into modifications of the observed brightness pattern. Studies can thus be performed in real time during ongoing catalytic reactions with the help of video techniques. The nanoscale resolution of FEM provides in this way information about the local surface composition and its variation over time. The microscope can be used to study the dynamics of non-equilibrium reactive systems at the nanoscale, by running it as an open chemical reactor with a constant pressure of gas-phase reactants and a controlled temperature. When bringing such a system far from thermodynamic equilibrium, nonlinear dynamics like explosive behaviors and periodic oscillations may emerge.[10,11]

The present paper is focused on the nonlinear behaviors occurring on the surface of a nanosized Pt sample put in contact with NO_2 and H_2 gases. This reactive system was shown to feature complex dynamical phenomena, including unimodal and multimodal periodic oscillations.[4,12–15] The emergence of such behaviors is usually rationalized in terms of nonlinear deterministic evolution equations for the chemical species involved. This approach allows for the identification of bifurcations, which signal the occurrence of qualitative changes in the nature of the attractors underlying the kinetics of the system. However, the small size of the samples used in FEM has the consequence that the dynamics of the system is strongly affected by fluctuations. Under such circumstances, the traditional concepts and objects appearing in a deterministic modelling approach need to be replaced by their stochastic counterparts.

In this work, we combine real-time FEM measurements of the chemical activity at the nanometric scale with nonlinear time series analyses to detect bifurcations and reconstruct the probability distribution of fluctuations around the

---

[a] *Chemical Physics of Materials and Catalysis, Université Libre de Bruxelles (ULB), CP243, 1050 Brussels, Belgium. E-mail: cbarroo@ulb.ac.be*
[b] *Interdisciplinary Center for Nonlinear Phenomena and Complex Systems (CENOLI), Université Libre de Bruxelles (ULB), CP231, 1050 Brussels, Belgium*
[c] *NonLinear Physical Chemistry Unit, Université Libre de Bruxelles (ULB), CP231, 1050 Brussels, Belgium*

underlying attractor. For the sake of brevity, we will name the structure defined in this way a ''stochastic attractor''. We show in particular that the observed oscillations can be related to the presence of a crater in the probability distribution of the system's state, as predicted by stochastic theories of reactive systems. The reconstruction of attractors allows for an estimation of the dimensionality of the system's deterministic ''backbone'' and of the degree of dispersion of trajectories around this deterministic state of reference. The conclusions drawn from data analyses are additionally supported by a stochastic model for the reactions taking place on the sample.

The paper is organized as follows. In Section II, we provide details on the experimental setup and on the procedure used to extract the time series. Section III is devoted to a presentation of the main dynamical features associated with the system. The phase space reconstructions are presented in Section IV. We discuss and present a simple chemical mechanism in Section V, in which we also compare the predictions of this model to the results of data analyses. We finish with a short summary and a discussion on possible extensions of this work (Section VI).

II Methods

The experiments were carried out in a stainless-steel field ion/electron microscope with a base pressure of 10^{-7} Pa. Details on the setup and principles of the methods can be found elsewhere.[16] The platinum field emitter tips, used as model catalysts, were electrochemically etched in a molten salt mixture of NaCl/$NaNO_3$ (1 : 4 w/w). The samples were then cleaned *in situ* by cycles of treatments consisting of field evaporation, annealing and ion sputtering.[13] The tips were eventually characterized with atomic lateral resolution by field ion microscopy (FIM) at 60 K.

The microscope can be operated either in a FIM, or in a FEM mode. FIM provides atomic lateral resolution of the tip but requires high electric fields ($\geq$10 V nm^{-1}) for the ionization of the imaging species. The use of large electric fields can represent an important drawback for the monitoring and analysis of chemical reactions. Strong electric fields are known to affect processes such as chemisorption and surface mobility. They can also modify the binding energies of adsorbates and thus the rate and/or mechanism of surface reactions.[17–19] They moreover cause mechanical strains that can make the tip fracture, which leads to the destruction of the whole sample. To overcome such difficulties, the FEM mode was preferred in this study since FEM requires electric fields up to ten times less than those used in FIM.

The sample was heated to 390 K and a field of 4–5 V nm^{-1} was applied, which is sufficient for image formation to occur. A mixture of nitrogen dioxide (purity 98.0%) and dihydrogen (purity 99.9996%) was then admitted into the chamber at pressures ranging from 10^{-5} to 5×10^{-2} Pa and the ongoing reaction was followed by video-recording the screen of the microscope. The time resolution of the video camera was 40 ms. As mentioned in the Introduction, the local variations of the work function ϕ result in a dynamical brightness pattern on the screen because the intensity of the emitted current decreases exponentially with this quantity.[5,6] The average work function of Pt is ϕ = 5.3 eV.[20,21] Introducing hydrogen in the reaction chamber at 390 K does not change the work function,[22] but the presence of oxygen species, resulting from NO_2 dissociative adsorption, leads to an increase $\Delta\phi$ = +1 eV at 400 K on {111} and {001} facets[21] and thus to a darkening of the FEM pattern. It has been suggested that NO_2 hydrogenation is accompanied by the formation of H_2O.[13,15] Adsorbed water molecules are known to decrease the work function on Pt, with $\Delta\phi$ = −1.02 eV at 77 K,[23] which results in a brighter image. The dynamics of the process was analyzed by measuring the variations of brightness in time, image by image. In the case of an 8-bit coding, the brightness range spans over 256 shades of gray.

Fig. 1a shows a field ion micrograph of a pure platinum sample at 60 K. The most protruding atoms appear as white dots and selected planes are indicated by their Miller indices. Fig. 1b corresponds to the same sample imaged by FEM at 390 K during the $NO_2 + H_2$ reaction. The magnifications in FIM and FEM modes are identical and the identification of the different crystallographic orientations performed in FIM can be used to interpret the FEM images. A convenient way to do so is to invert the gray scale of the FEM pattern and to superimpose it on a FIM image, as shown in Fig. 1c. The resulting image

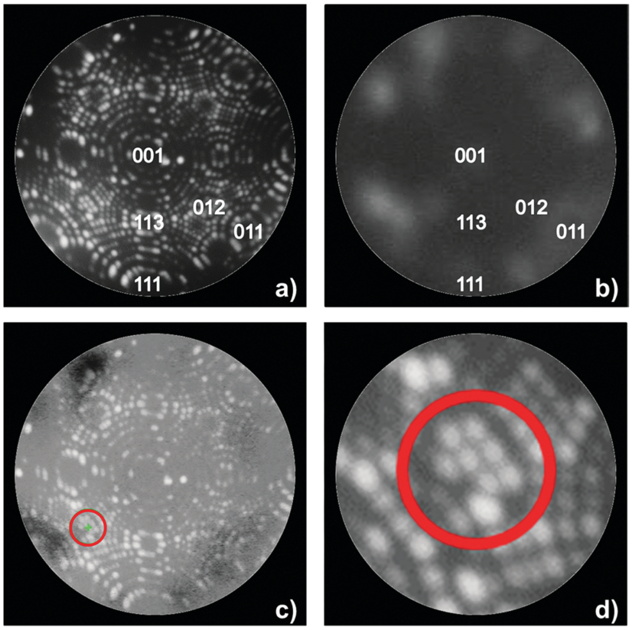

Fig. 1 (a) Field ion microscopy pattern of a pure platinum sample at cryogenic temperature with atomic resolution (temperature T = 60 K, neon pressure $P_{Ne} = 2 \times 10^{-3}$ Pa, electric field at the apex: $F \approx 35$ V nm^{-1}); (b) field emission microscopy pattern during reaction between NO_2 and H_2 (T = 390 K, $F \approx 4$ V nm^{-1}, $P_{NO_2} = 3.64 \times 10^{-4}$ Pa, $P_{H_2} = 1.05 \times 10^{-2}$ Pa); (c) superimposition of FIM and FEM patterns. The circle indicates a typical region of interest (ROI) subject to brightness monitoring; (d) magnification of one of the probed regions, corresponding to a (012)-type facet with an area of ~8 nm^2.

shows the correspondence between the two patterns and highlights the region for which we decided to monitor the brightness with a dedicated software.[24] A typical region of interest (ROI), which covers a {012} region of the sample, is indicated with a red circle in Fig. 1c and is magnified in Fig. 1d.

This family of facets has been determined to act as the pacemakers of the NO_2 + H_2 reaction on Pt tips.[25,26] Recent work also showed that these facets do not undergo reconstruction or restructuration,[12] which makes the interpretation of the changes in brightness easier since the local morphology of the sample (and hence the local electric field) remains so to say constant. There are approximately 40–45 surface atoms in this ROI. Taking into account the fcc structure and lattice parameter of Pt, the probed area can be shown to cover ≈ 8 nm^2.

III Local dynamics on relevant regions of interests

In this section, we briefly recall the main dynamical features associated with the NO_2 + H_2/Pt system hereby studied. The interested reader can refer to ref. 13–15 for a more detailed description of this reactive system. We studied NO_2 hydrogenation on the apex of a single platinum tip with a radius of curvature of ~ 20 nm. Maintaining a constant NO_2 pressure in the 10^{-4} Pa range, the pressure of H_2 was raised from 10^{-6} Pa to approximately 10^{-2} Pa. This increase revealed the existence of two main dynamical regimes. At low H_2 pressures, the brightness of the image in the ROI fluctuates around a low, constant value. The low brightness has been attributed to the presence of large amounts of adsorbed species O(ads) and/or NO_2(ads), which tend to increase the work function and thus to decrease the intensity of the emitted current.[8] Increasing the H_2 pressure leads to stronger fluctuations until a critical value $P^{c}_{H_2}$ is reached, above which self-sustained oscillations are observed (Fig. 2a). These oscillations correspond to a periodic alternation between states of low and high brightness. The rapid increase of brightness emerging from the dark background has been attributed to a fast water formation process.[9] The periodic character of the dynamics could be confirmed with Fourier power spectra of the time series (Fig. 2b), which show a well-defined frequency of 0.328 Hz for the depicted example.

To further characterize the properties of the fluctuation-perturbed oscillations, we also computed the normalized autocorrelation function

$$C(t - t_0) = \frac{\langle B(t)B(t_0)\rangle - \langle B(t)\rangle\langle B(t_0)\rangle}{\langle B^2(t_0)\rangle - \langle B(t_0)\rangle^2}$$

where B is the brightness of the signal, $t - t_0$ is a time interval and the brackets stand for averaging over the time of reference t_0. The autocorrelation function of the signal provides interesting information on the robustness of oscillations (Fig. 2c) since it measures the degree of linear correlation between two of the system's states as a function of the delay.[27,28] The fact that the autocorrelation function shows damped oscillations with an envelope extending over several periods means that oscillations taking place successively are highly correlated, while those separated by large delays are only poorly correlated. In the case of Fig. 2c, the half-time of the envelope of these oscillations $t_{1/2}$ is close to 10 periods (see the red line). The unexpected regularity of this phenomenon could be traced back to a strong spatial coupling involving the propagation of ultrafast chemical waves across the tip.[15]

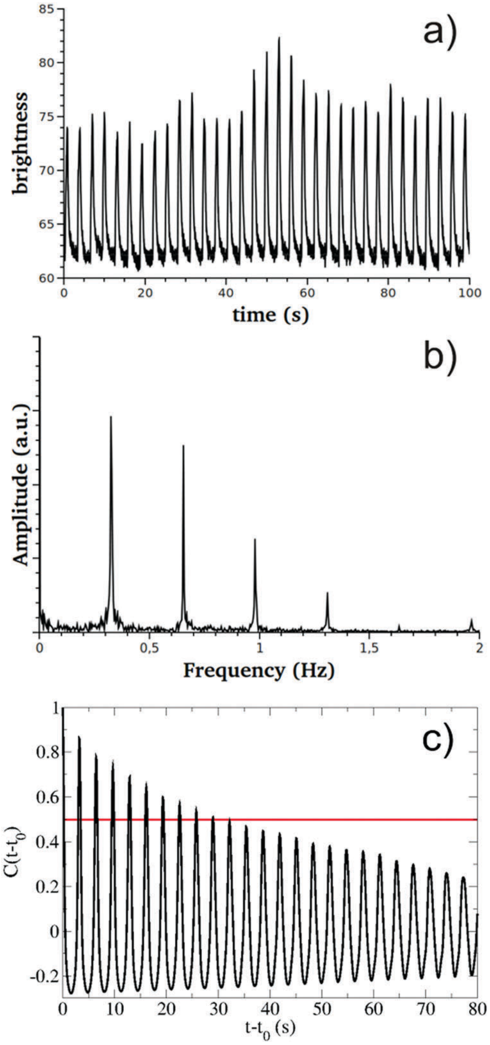

Fig. 2 (a) Time series of the brightness during self-sustained periodic oscillations. The conditions are: T = 390 K, $F \approx 4$ V nm^{-1}, $P_{NO_2} = 3.64 \times 10^{-4}$ Pa, $P_{H_2} = 1.05 \times 10^{-2}$ Pa; (b) Fourier power spectrum of this time series showing a well-defined base frequency of 0.328 Hz; (c) interval-dependent autocorrelation function. The red line indicates when the envelope of the damped oscillations reaches half of its initial value.

The change from the steady-state to the oscillating regimes can be summarized in a bifurcation diagram. Fig. 3 plots the average frequency of oscillations as a function of P_{H_2} for a fixed pressure of NO_2 at 390 K. The frequency is zero for the steady-state found at low P_{H_2} and it is seen to increase with this pressure after the bifurcation point $P^{c}_{H_2}$ has been crossed. The increase in frequency was shown to be consistent with the occurrence of an infinite period bifurcation.[14] Due to technical limitations, the H_2 pressure cannot be increased beyond the last point shown in

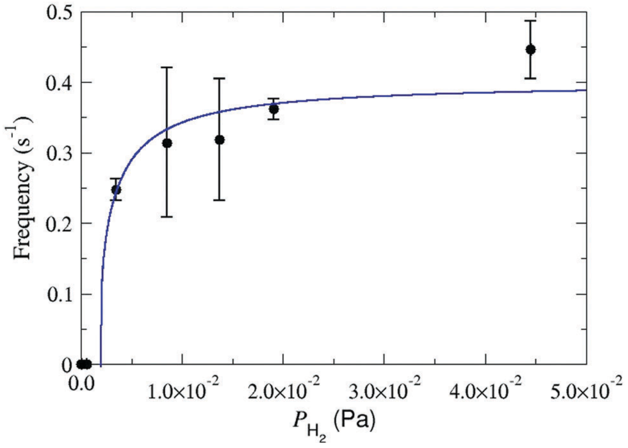

Fig. 3 Frequency of oscillations as a function of the H_2 pressure. All other parameters are the same as in Fig. 2. The blue line is a power law corresponding to an infinite period bifurcation (see ref. 14 for a more detailed discussion on the bifurcation involved). Adapted with permission from ref. 14. Copyright 2015 American Chemical Society.

this figure but experiments performed under slightly different conditions (at a lower base pressure of NO_2) indicate that the frequency tends to saturate and subsequently decrease for larger P_{H_2} values. The amplitude of oscillations, on the other hand, does not show any specific trend. Oscillations present a rather large amplitude as soon as the bifurcation is crossed, and this amplitude remains more or less constant, irrespective of the distance from $P^{c}_{H_2}$.

IV Dynamical attractors

An alternative and more revealing way of characterizing a nonlinear dynamical system is to analyze the properties of the attractor(s) corresponding to the observed dynamics. If our observations indeed correspond to fluctuations-perturbed self-sustained oscillations, one should be able to reconstruct trajectories in the phase space spanned by the variables controlling the dynamics and verify that they define an underlying limit cycle.[29]

It is however often impossible to access the "true" phase space and attractors of a system since all these variables are not accessible.[30] It was shown that the most important topological properties of attractors are conserved when using, instead of the "true" state variables, new coordinates corresponding to delayed time series of a single measurement,[31–33] This technique is known as the time-delay embedding method. We thus define a collection of vectors $B(t)$, $B(t+\tau)$, $B(t+2\tau)$,…$B(t+(d_E-1)\tau)$, where $B(t)$ stands for the brightness measured at time t and τ is a delay, and will construct a phase space on this basis. Important parameters in this approach are the value of the delay and the number of delayed time series to be retained, which defines the dimensionality, or more precisely the embedding dimension d_E, of the reconstructed phase space. This embedding dimension represents the dimensionality of the space in which the attractor can be fully embedded.

To determine the optimal delay, we calculated the average mutual information (AMI). The AMI is a measure of the degree of correlation between measurements taken at different times. The first minimum of the AMI as a function of the time difference often provides a good choice for the delay, which can then be used to estimate the embedding dimension. We determined the optimal embedding dimension with the false nearest neighbors (FNN) method.[34] The FNN method is based on finding data points that are close in a space of dimension N and on verifying if they remain close in a space of dimension $N+1$. If they do not remain close to each other, these data points are considered as "false neighbors". The procedure is iterated until the fraction of false neighbors converges to a minimum and the corresponding dimension is considered to be the optimal embedding dimension d_E. Other approaches, including calculations of the correlation dimension, did not lead to convergent (or meaningful) results because of the background noise. The AMI and FNN analyses were performed with the TISEAN 3.0.1 package for nonlinear time series analyses.[35] More details on the use of these techniques for the analysis of nanoscale systems can be found in ref. 36.

Table 1 summarizes the values of the embedding dimension for the reported oscillations. We obtained a value of d_E comprised between 3 and 5 (with $d_E = 4$ for the example shown in Fig. 2), which suggests that the dimension of the attractor is smaller or equal to 5. For a limit cycle, an embedding dimension of 2 is sufficient since the attractor itself is 1-dimensional but noise is often observed to lead to higher dimensions with the FNN technique. In our case, similar dimensions were obtained when the high-frequency background noise of the original signal had been filtered out (with a low-pass filter or with the linear noise reduction data processing tool in *TISEAN*). This result indicates that the high dimensionality we obtained is not a consequence of the rapid fluctuations of low amplitude but rather of the variability of the amplitude of oscillations (the period being usually very well-defined), which cannot be removed with simple noise reduction techniques.

This can be confirmed by analyses done on a "mean" time series obtained by performing a periodic averaging procedure, in which the original time series are divided into boxes whose size is equal to the mean period and from which a mean

Table 1 Pressures of the NO_2 and H_2 reactants, optimal delay (τ) obtained with the AMI and embedding dimension d_E as determined by the FNN method in the case of oscillating dynamics (see text for more details). The Theiler window was taken in each case to be equal to $3t_{1/2}$ (the half-time of the autocorrelation function)

P_{NO_2} (Pa)	P_{H_2} (Pa)	τ (s)	d_E
5.36×10^{-4}	1.57×10^{-2}	1.12	5
5.36×10^{-4}	2.41×10^{-2}	0.92	4
5.43×10^{-4}	4.45×10^{-2}	0.60	5
5.43×10^{-4}	1.91×10^{-2}	0.80	5
5.43×10^{-4}	3.48×10^{-3}	2.00	5
3.64×10^{-4}	1.05×10^{-2}	0.40	4
3.64×10^{-4}	1.46×10^{-2}	0.40	5
3.64×10^{-4}	2.10×10^{-2}	0.60	3
3.64×10^{-4}	4.00×10^{-2}	0.80	4
2.16×10^{-4}	2.00×10^{-2}	1.20	5
2.16×10^{-4}	2.18×10^{-2}	1.80	5
2.16×10^{-4}	2.44×10^{-2}	2.44	4

oscillation is obtained by averaging the signal over all these boxes. With such a mean, representing the deterministic backbone of the oscillations, we found $d_E = 2$ in all cases. This suggests that the underlying deterministic attractor is 1-dimensional (fractal dimensions can be ruled out since the mean oscillations do not show any sign of chaotic behavior).

It is instructive to show how the signal trajectories fluctuate around the mean cycle (as defined above). The values of the embedding dimensions obtained for the original time series suggest that fluctuations around the mean attractor can be embedded in a space whose dimension ranges between 3 and 5. For visualization purposes, we will here show 2-dimensional projections of these spaces. Fig. 4 plots such a 2-dimensional phase space for the time series of Fig. 2, for which the optimal delay is τ = 400 ms. The mean oscillation is depicted in red and the black arrows are the velocities of trajectories. These vectors were calculated by regrouping trajectory points into 2-dimensional bins (whose size was determined by the square-root law) and by calculating the average motion in phase space from all the points in each box. The vector field constructed in this way shows that the amplitude of the signal can sometimes strongly vary: fluctuations transversal to the limit cycle may be as large as the limit cycle itself. On the other hand, we already mentioned that the period is well-defined and fluctuates only slightly. This robustness can be seen a consequence of the attracting character of the underlying cycle, as witnessed here by the fact that points located far from the cycle are strongly attracted by it (the local speed is large). Similar characteristics, namely robust periods with highly fluctuating amplitudes, were observed for model chemical oscillators with strong nonlinear feedback.[37]

Phase space reconstruction can also be used to evaluate the probability distribution of trajectories around the deterministic attractors. The histograms shown in Fig. 5a were built from the trajectories in phase space corresponding to time series taken for parameter values where no oscillations are seen. We used the delay and the dimension obtained for the oscillations to reconstruct the phase space for this steady state as well.

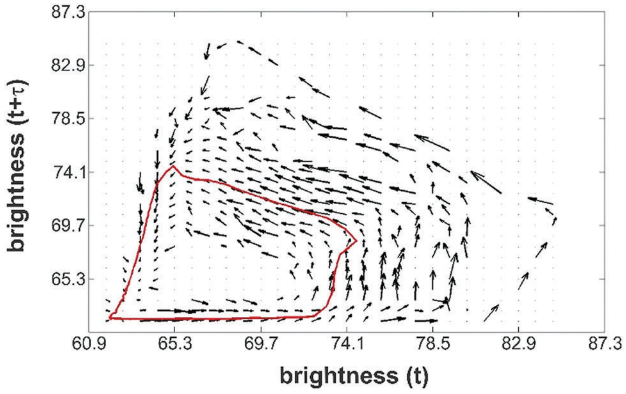

Fig. 4 Average dynamical attractor, reconstructed from the time series in Fig. 2 as obtained with the delay-embedding method (with τ = 400 ms) (in red). The vector field is also represented highlighting the fluctuations in amplitude of the dynamics, as well as the trajectories around the limit cycle.

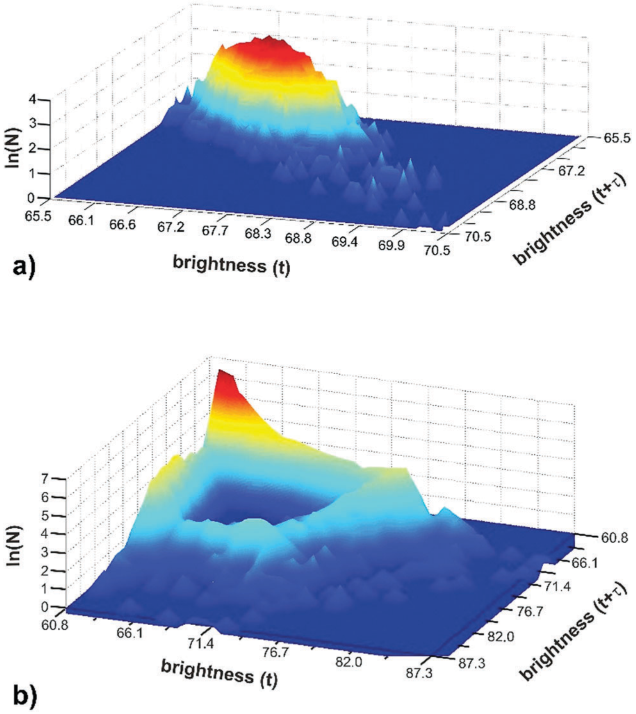

Fig. 5 3-Dimensional histograms reconstructed from the time series (a) of the steady state before the bifurcation point (P_{H_2} = 1.18 × 10^{-3} Pa) and (b) of the oscillations presented in Fig. 2. All the other parameters are the same as before and the time delay τ is the same as in Fig. 4. A color scale was used to distinguish more easily states of high probability (red) from low-probability states (blue). A smoothing (spline) of the histograms has been applied for the sake of presentation.

The reconstructed space is divided into boxes and the logarithm of the number of phase space points in each box is plotted on the vertical axis. In the absence of oscillations, the system is characterized by a one-humped probability distribution centered on a single value corresponding to the mean of the signal.

This shape is characteristic of fluctuations around a stable steady state. It drastically changes when oscillations appear (see Fig. 5b): after the bifurcation point, the trajectories define a crater-like structure whose rim corresponds to the mean limit cycle and whose slopes are shallow in the zones of large deviations from the cycle and are steep whenever trajectories tend to concentrate close to it. These properties are those expected in the case of a noise-perturbed dynamical system having a periodic deterministic backbone. To the best of our knowledge, these results represent the first experimental evidence of the existence of such stochastic attractor at the nanoscale.

V Kinetic model

The shape of the stochastic attractors presented in the previous section points to the idea that the observed phenomena correspond to a nonlinear dynamical system perturbed by noise. In view of the properties of the system at hand, we expect this noise to be of molecular origin. In this section, we present and analyze the most relevant features of a model for the reaction under consideration. Our main objective will be to identify the source of nonlinearities and to confirm the origin of the noise affecting the system's dynamics.

V.a Reaction mechanism

The core of the reaction is expected to correspond to a Langmuir–Hinshelwood type of process. Accordingly, we suppose that the two reactants adsorb from the gas phase following the elementary steps:

$$\mathrm{NO_2(g)} + x\mathrm{S} \rightleftarrows \mathrm{NO_2(ads)} \tag{1}$$

$$\mathrm{H_2(g)} + 2\mathrm{S} \rightleftarrows 2\mathrm{H(ads)} \tag{2}$$

In these equations, S stands for an empty surface site and (g) and (ads) refer to gas-phase and adsorbed species, respectively. Here, we used the fact that the adsorption of H_2 is known to be dissociative on most Pt facets at the temperature of interest. Studies performed with density functional theory (DFT) calculations suggest on the other hand that the adsorption of NO_2 can be molecular.[38] The stoichiometry of degree $x \geq 2$ used in eqn (1) is representative of the idea that a single adsorbed NO_2 molecule can block several adsorption sites.[28]

Next, we include the fact that the molecularly adsorbed NO_2 species can subsequently decompose into NO and O:

$$\mathrm{NO_2(ads)} + y\mathrm{S} \rightarrow \mathrm{NO(ads)} + \mathrm{O(ads)} + (x - 2 + y)\mathrm{S} \tag{3}$$

We consider this step to be irreversible since the formation of NO_2 from NO and O on Pt is very unlikely at 400 K.[38] It was shown by DFT calculations that the decomposition of NO_2 on Pt requires at least one empty surface site,[28] so that $y \geq 1$. The exact dependence of the NO_2 dissociation probability on the fraction of available active sites is not known. In view of its adsorption geometry,[28] we should expect however that the dissociation of NO_2 becomes strongly hindered when the fraction of empty sites decreases below a given critical value.

We also take into account the possibility for the released NO to either desorb or dissociate,

$$\mathrm{NO(ads)} \rightarrow \mathrm{NO(g)} + \mathrm{S} \tag{4}$$

$$\mathrm{NO(ads)} + z\mathrm{S} \rightarrow \mathrm{N(ads)} + \mathrm{O(ads)} + (z - 1)\mathrm{S} \tag{5}$$

Re-adsorption of NO can safely be neglected since NO(g) is produced in small amounts and since the gas phase is subjected to continuous pumping. Previous kinetic models for the decomposition of NO,[39] as well as DFT studies performed on surfaces with various crystallographic orientations,[40] indicate that the decomposition of NO is irreversible and is such that $z \geq 1$. The final steps of the model include reactions between adatoms to give water and N_2, respectively

$$\mathrm{O(ads)} + 2\mathrm{H(ads)} \rightarrow \mathrm{H_2O(g)} + 3\mathrm{S} \tag{6}$$

$$2\mathrm{N(ads)} \rightarrow \mathrm{N_2(g)} + 2\mathrm{S} \tag{7}$$

These reactions are irreversible because the partial pressures of H_2O(g) and N_2(g) are kept negligible by the continuous pumping. Both N_2 and H_2O have extremely short lifetimes on Pt at 400 K, so that we do not need to consider the adsorbates H_2O(ads) and N_2(ads). The reaction (7) is supposed to be fast in order to prevent the formation of NH_x species, which are not observed in the experiments. Note that the steps (1)–(7), on which we base our model, are a simplification of a more general double-path mechanism developed earlier for this reaction.[13]

V.b Mean-field properties

To quantify the deterministic kinetics associated with steps (1)–(7), we consider the time evolution of the coverages $[\mathrm{X}] = N_\mathrm{X}/\Omega$, where N_X stands for the number of adsorbed particles of a given species and Ω represents the constant total number of available active sites. In the limit of homogeneous ideal systems, the evolution equations for these variables read:

$$\frac{\mathrm{d}[\mathrm{NO_2}]}{\mathrm{d}t} = k_1[\mathrm{S}]^x - k_{-1}[\mathrm{NO_2}] - k_3[\mathrm{NO_2}]G([\mathrm{S}]) \tag{8}$$

$$\frac{\mathrm{d}[\mathrm{NO}]}{\mathrm{d}t} = k_3[\mathrm{NO_2}]G([\mathrm{S}]) - k_4[\mathrm{NO}] - k_5[\mathrm{NO}][\mathrm{S}]^z \tag{9}$$

$$\frac{\mathrm{d}[\mathrm{O}]}{\mathrm{d}t} = k_3[\mathrm{NO_2}]G([\mathrm{S}]) + k_5[\mathrm{NO}][\mathrm{S}]^z - k_6[\mathrm{O}][\mathrm{H}]^2 \tag{10}$$

$$\frac{\mathrm{d}[\mathrm{H}]}{\mathrm{d}t} = 2k_2[\mathrm{S}]^2 - 2k_{-2}[\mathrm{H}]^2 - 2k_6[\mathrm{O}][\mathrm{H}]^2 \tag{11}$$

$$\frac{\mathrm{d}[\mathrm{N}]}{\mathrm{d}t} = k_5[\mathrm{NO}][\mathrm{S}]^z - 2k_7[\mathrm{N}]^2 \tag{12}$$

Note that in the type of experiments we are modelling here, the temperature of the solid substrate and in the gas phase can be considered constant. In the above equations, the concentration in empty sites is given by $[\mathrm{S}] = 1 - x[\mathrm{NO_2}] - [\mathrm{NO}] - [\mathrm{O}] - [\mathrm{H}] - [\mathrm{N}]$ and k_i (k_{-i}) is the reaction rate constant of step i (and its reverse $-i$). The pressures of NO_2(g) and H_2(g) are included in the kinetic constant k_1 and k_2 respectively (see Table 2). To take into account the strong dependence of NO_2 dissociation on [S], we introduce a Heaviside-type function $G([\mathrm{S}])$ such that

$$\begin{aligned} G([\mathrm{S}]) &= [\mathrm{S}]^y \quad \text{when } [\mathrm{S}] \geq [\mathrm{S}]_\mathrm{crit} \\ &= 0 \quad\quad\;\; \text{otherwise} \end{aligned}$$

Note that this is a standard way to model surface processes characterized by a critical concentration.

The above system of equations can be further simplified. We first note that the coverage in nitrogen adatoms [N] is expected to be very low since $k_7 \gg k_5$ on Pt at the temperature of interest (see, for example ref. 39 and 40) and we thus neglect this quantity. Second, we can take advantage of the fact that oscillations are observed at high $P_{\mathrm{H_2}}/P_{\mathrm{NO_2}}$ ratios so that k_2 is much larger than k_1. Since the rate constants for the desorption of H_2 and for the formation of water are also large at $T \approx 400$ K, the coverage [H] involves fast processes only and can be evaluated by adiabatic elimination (*i.e.*, by setting $\mathrm{d}[\mathrm{H}]/\mathrm{d}t = 0$):

$$[\mathrm{H}]^2 \approx \frac{k_2}{k_{-2} + k_6[\mathrm{O}]}[\mathrm{S}]^2$$

Table 2 Numerical values for the parameters used in eqn (13)–(15). The values of k_1 and k_2 were calculated by multiplying the hitting frequency from the kinetic theory of gases by an initial sticking coefficient of 0.9 for NO_2 (a value close to that of NO) and of 0.2 for H_2[41]

Kinetic constant	Pre-exponential factor (s^{-1})	Activation energy (kJ mol^{-1})	Value at 390 K (s^{-1})	Source
k_1	$1.52 \times 10^3\ P_{NO_2}$	—	—	This work
k_{-1}	—	—	3.5	This work
k_2	$1.66 \times 10^3\ P_{H_2}$	—	—	Ref. 41
k_{-2}	1.0×10^{12}	104.5	9.8×10^{-3}	Ref. 39 – Pt(100)
k_3	1.0×10^{13}	49.1	2.7×10^6	Ref. 28 – Pt(100)
k_4	1.0×10^{15}	146.5	2.4×10^{-5}	Ref. 40
k_5	1.0×10^{13}	107.1	4.5×10^{-2}	Ref. 40
k_6	1.0×10^{13}	54.34	5.3×10^5	Ref. 28 – Pt(100)

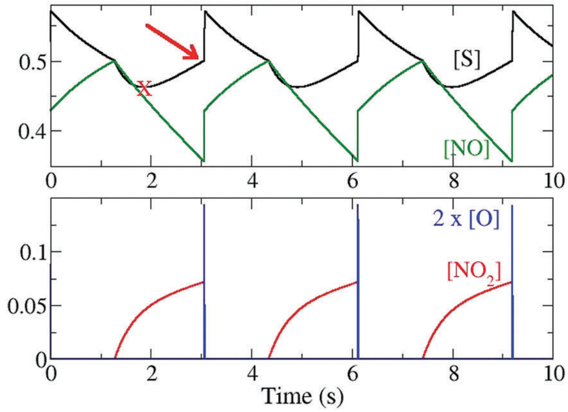

Fig. 6 Time series of the coverages, obtained by numerical integration of eqn (13)–(15) with a time step dt = 10^{-8}. The initial condition was [NO] = 0.4, [NO_2] = 0.2, [O] = 0. $[S]_{crit}$ = 0.5. The pressures are the same as in Fig. 2. Other parameter values are given in Table 2.

The mean-field evolution equations for the model under consideration thus finally read

$$\frac{d[NO_2]}{dt} = k_1[S]^x - k_{-1}[NO_2] - k_3[NO_2]G([S]) \tag{13}$$

$$\frac{d[NO]}{dt} = k_3[NO_2]G([S]) - k_4[NO] - k_5[NO][S]^z \tag{14}$$

$$\frac{d[O]}{dt} = k_3[NO_2]G([S]) + k_5[NO][S]^z - \frac{k_2k_6}{k_{-2}+k_6[O]}[O][S]^2 \tag{15}$$

With [S] = 1 − x[NO_2] − [NO] − [O]. Eqn (13)–(15) were numerically integrated with a 4th-order Runge and Kutta method whose time step dt was typically comprised between 10^{-7} and 10^{-9} s. The values of the parameters used are given in Table 2. Most parameters correspond to values for {210} facets. When these quantities were not available, values for Pt(001) were considered instead. This choice is motivated by the fact that experiments performed under slightly different conditions led to oscillations involving the central (001) facet of the samples, indicating that the kinetic conditions are similar for both orientations.[28] We considered x = 2 and y = z = 1 for simplicity but that qualitatively similar results are obtained for larger values of these orders of reaction. The NO_2 desorption rate constant (k_{-1}) was used as fitting parameter, since there is little information in the literature concerning this quantity.

Numerical integrations reveal that the model presents self-sustained oscillations of the coverages for a wide range of parameters in agreement with experimental data. Moreover, the frequency of the oscillations matches those of the experiments. An example of such oscillation is given in Fig. 6.

A single oscillation cycle can be decomposed into three main stages. To fix ideas, we start from the state depicted by a cross in Fig. 6. In this first stage, the surface is highly covered ([S] is at its lowest) so that NO_2 can adsorb molecularly but cannot dissociate. This leads to a slow buildup of the corresponding coverage, [NO_2]. The absence of NO_2 decomposition also has the consequence that there is no more source of NO(ads), whose coverage decreases as a consequence of desorption and decomposition of this species. Since during the same period of time [O] remains low, the concentration in empty sites slowly increases until it reaches the critical value at which NO_2 decomposition is activated (see the arrow in Fig. 6). Once this threshold has been crossed, a second phase is initiated in which large amounts of NO(ads) and O(ads) are deposited on the surface as a consequence of the rapid decomposition of NO_2. The simultaneous disappearance of NO_2 and rapid removal of O through water formation lead to a rapid increase of the number of empty active sites. However, the decomposition of NO_2 also releases NO species which are not rapidly removed from the surface. This leads to a third phase of the oscillations where NO slowly builds up so that the number of available empty sites decreases and, eventually, goes below its critical value again so that a new cycle can begin.

In order to allow for a more direct comparison with experimental results, numerical integrations can also be used to predict the time evolution of the electronic current, which we expect to be proportional to the recorded brightness level. In its simplest form, the Fowler–Nordheim theory predicts that the amplitude I of the emission current is given by[6]

$$I = Aa\phi^{-1}F^2 \exp\left(-\frac{b\phi^{3/2}}{F}\right) \tag{16}$$

where A is the area of emission, F the external electric field intensity, ϕ the local work function; $a = 1.5414\ldots \times 10^{-6}$ A eV V^{-2} and $b = 6.8309\ldots \times 10^9$ $eV^{-3/2}$ V m^{-1} are universal constants. Since experiments reveal no sign of the presence of surface reconstructions we can consider A and F to be constant. The local work function is on the other hand expected to depend on the local coverages and thus to vary in time. To take this into account we consider that ϕ varies linearly with the coverages:

$$\phi = \phi_0 + \alpha[NO_2] + \beta[NO] + \gamma[O] \tag{17}$$

In this equation, ϕ_0 = 5.35 eV is the work function of a clean Pt(210) facet. The correction factor γ is estimated to be ≈1.5 eV based on measurements of electron emission intensity in photoelectron emission microscopy experiments performed on Pt(110)

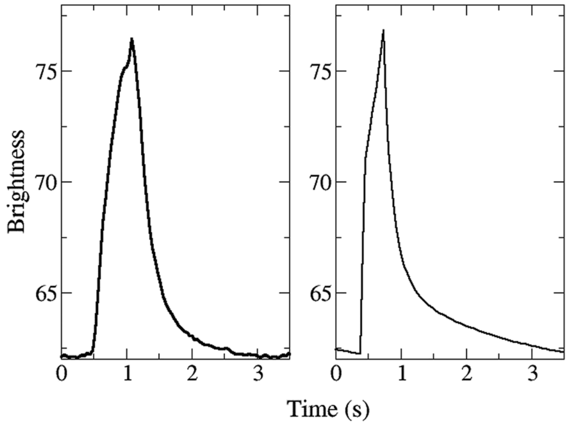

Fig. 7 Left hand side: Brightness peak as obtained by performing a periodic averaging of oscillations reported in Fig. 2. Right hand side: Rescaled current peak obtained with eqn (16) with $F = 4\ \mathrm{V\ nm^{-1}}$, $\alpha = 1.0$ eV, $\beta = -0.75$ eV and $\gamma = 1.5$ eV. The factor before the exponential has been chosen so as to match the brightness amplitude, and the whole signal was translated to account for the baseline of the brightness signal.

(whose work function is close to that of Pt(210)).[42] The values of α and β are not known and were used to fit the shape of the experimental brightness peaks. The best fit was obtained by taking positive values for α and negative values for β. This suggests that molecularly adsorbed NO_2 tends to increase the work function (and thus to decrease brightness) while NO has an opposite, but less pronounced effect. With the chosen values, the intensity of the current predicted by the model combined with the Fowler–Nordheim equation bears strong similarities with the brightness signal, as can be seen in Fig. 7, where the mean-field prediction is plotted alongside a time-averaged oscillation peak obtained from experiments. In particular, both the experiments and the model predict a rapid increase of brightness in the first stage of the oscillations, followed by a much slower relaxation towards the initial state.

To summarize, the reaction model that we propose here is able to predict the existence of oscillations (and thus of a limit cycle) leading to periods and amplitudes of the brightness signal that compare well with experiments. This supports the idea that experimental observations correspond to oscillations of chemical origin. One should however keep in mind that the proposed reaction scheme is probably a very simplified picture of the processes taking place in experiments. In particular, the model rests on the idea that the H_2 pressure is large enough. Consequently, it correctly predicts that the frequency of oscillations increases slowly with the H_2 pressure and saturates for large P_{H_2} (not shown here), as observed in experiments. However, for too low H_2 pressures the predictions of the model start to deviate from observations. We observe for example that in the model the frequency first decreases as P_{H_2} is lowered, as expected, but then starts increasing again because of the appearance of fast, very low amplitude oscillations. While developing a more detailed model would certainly be illuminating, for example to verify the type of bifurcation taking place, our main focus here is on the role of fluctuations on the oscillations that are observed far from the bifurcation point (*i.e.*, in the domain of validity of the model). We will thus instead focus now on the predictions of a stochastic implementation of the reaction processes.

V.c The role of fluctuations

In view of the small size of the system involved, fluctuations of the surface composition are expected to play an important role. We take this into account by modelling the different reactions as Markovian birth-and-death processes for the number of particles of each species (N_{NO_2}, N_{NO} and N_O), still considering that the other state variables (such as the pressures and temperature) remain constant. The probability $P(\boldsymbol{N},t)$ to find the system in a state $N = (N_{NO_2}, N_{No}\ N_O)$ at time t obeys the chemical master equation:

$$\frac{\mathrm{d}}{\mathrm{d}t}P(\boldsymbol{N},t) = \sum_i [W_i(\boldsymbol{N}|\boldsymbol{N}-\boldsymbol{\nu}_i)P(\boldsymbol{N}-\boldsymbol{\nu}_i,t) - W_i(\boldsymbol{N}+\boldsymbol{\nu}_i|\boldsymbol{N})P(\boldsymbol{N},t)] \tag{18}$$

where i stands for one of the elementary processes and ν_i is the associated vector of stoichiometric coefficients. The transition probabilities per unit time W_i are given in Table 3. The total number of active sites $\Omega = 2N_{NO_2} + N_{NO} + N_O + N_S$ plays the role of an extensivity parameter. Individual trajectories consistent with eqn (18) were generated with Gillespie's stochastic simulation algorithm and form the basis of our stochastic analysis.

Using parameter values given in Table 2, simulations show fluctuation-perturbed oscillations for a wide range of Ω values. The degree of regularity of these oscillations can be quantified by comparing the half-time $t_{1/2}$ of the envelope of the autocorrelation functions to the averaged period $\bar{T}$ (the mean first-return time) of the signal. By convention, "true" periodic behaviors are usually associated with situations where $t_{1/2} > \bar{T}$.[14,37,43] Simulations here show that this criterion is respected for $\Omega \gtrsim 10^2$, which is of the same order of magnitude as the value found for simple chemical and biochemical models.[37,43]

In order to estimate the value of the extensivity parameter corresponding to the experimental results considered here, we compared the temporal autocorrelation functions of the

Table 3 Transition probabilities per unit time for the different processes involved in the simplified model. The numerical values for the various parameters are the same as in Table 2 (except for Ω, see text). $N_S = \Omega - 2N_{NO_2} - N_{NO} - N_O$ stands for the number of available empty surface sites

Process	Transition probabilities per unit time (s^{-1})	
NO_2 adsorption	$k_1N_S(N_S-1)\Omega^{-1}$	
NO_2 desorption	$k_{-1}N_{NO_2}$	
NO_2 decomposition	$k_1N_{NO_2}(N_S-1)\Omega^{-1}$	if $[S] > 0.5$
	0	otherwise
NO desorption	k_4N_{NO}	
NO decomposition	$k_5N_{NO}(N_S-1)\Omega^{-1}$	
H_2O formation	$\dfrac{k_2k_6}{k_{-2}+\dfrac{k_6N_{NO}}{\Omega}}N_{NO}(N_S-1)(N_S-2)\Omega^{-2}$	

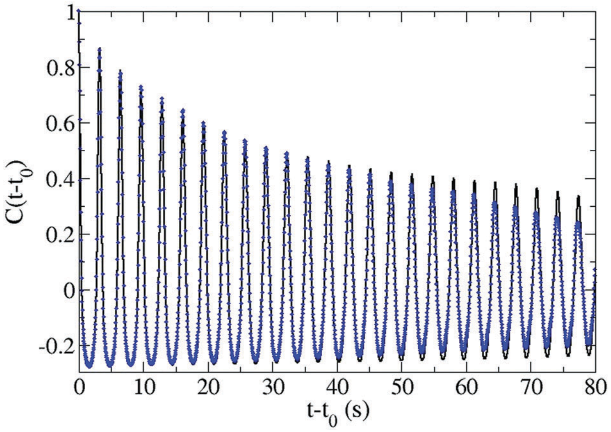

Fig. 8 Comparison between the experimental autocorrelation function $C(t - t_0)$ (blue dots) and the one obtained by stochastic simulations (black curve). Both curves are based on time series of the brightness. The experimental results correspond to the conditions of Fig. 2. The stochastic simulations were performed with the parameter values given in Table 2 and with Ω = 39 800 (the partial pressures are the same as in Fig. 2 as well).

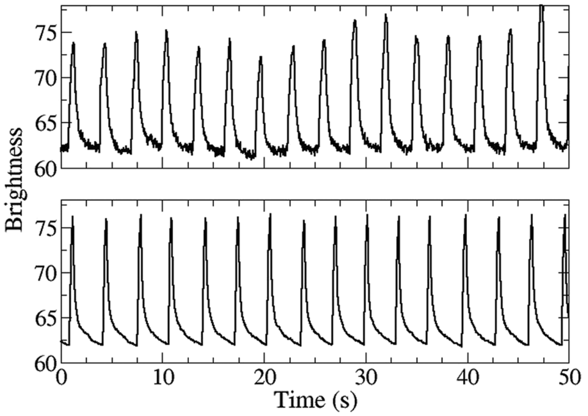

Fig. 9 Experimental (top panel) and theoretical (bottom panel) time series for the brightness of the signal. Experimental conditions and model parameters are the same as in Fig. 8.

brightness obtained with simulations to their experimental counterpart. Ω was then varied until the two curves match. Fig. 8 gives an example of such a ''correlation-based'' fitting procedure. For this particular example, we found $\Omega \approx 40\,000$ and similar values ($\Omega \approx 10^3$–10^4) were obtained for the other cases. It is interesting to compare these values with an estimation of the number of active sites in the ROI. The ROI has an area of $\simeq 8$ nm^2, which corresponds to approximately 40–45 active sites. However, we observed in the experiments that the 4 facets corresponding to the {012} orientation oscillate in an almost perfectly synchronous way.[15] This synchronization could be traced back to a fast propagation of waves across the sample that effectively couples the different regions of the tip.[15] It takes only about 20 milliseconds for the waves to propagate over the whole observable part of the sample. This suggests that with the time resolution used here, the observed dynamics would correspond to that of a ''homogeneous'' system comprising all the active sites of the sample. The field of view presented in Fig. 1 corresponds to only $\approx 10^3$ surface sites, but the accessible sample surface in FEM is usually estimated to be close to 2/3 of the area presented by the (almost) hemispherical apex. Using a curvature radius of $\approx$20 nm and the lattice constant of platinum leads to a total of about 10^4 surface sites, which is indeed close to the values we obtained for Ω by fitting the autocorrelation functions. This result points to the idea that parts of the surface that remain dark or cannot be observed in FEM could also be participating in the reaction.

Realizations of Gillespie's algorithm with the appropriate Ω values lead to oscillations having a fluctuating period and amplitude, in qualitative agreement with observations (see Fig. 9 for a comparison between experimental and theoretical time series). However, as can be noticed already by visual inspection of these time series, the amplitude fluctuates less in simulations than it does in experiments. This difference is also at the origin of discrepancies that start to appear between the theoretical and the experimental autocorrelation functions for long delays. This can be seen already in Fig. 8 where the experimental autocorrelation decreases faster than the theoretical one after $\approx$12–13 periods. There could be several reasons behind these differences. One possibility would be that molecular noise affects oscillations differently in the experiments and in the model. Indeed, in a recent paper,[44] Cosi and Krischer highlighted two paths to the loss of regularity in oscillations for the stochastic model of an electrochemical system. One of them corresponds to a strong variability of the amplitude, with a probability distribution of the first return times remaining more or less Gaussian. The other is characterized by strong fluctuations of the first return time, which reflects itself in the form of highly asymmetric probability distributions with pronounced long tails. In our case, the first return times of oscillations follow distributions that are highly symmetric and can be well fitted with a Gaussian curve, in the experimental case as well as for simulations. This seems to indicate that they both belong to the ''amplitude'' type and that the observed differences cannot be attributed to a different role played by fluctuations.

The ''missing noise'' could arise from additional reactive steps that were not included in the model, or could originate from local fluctuations in the partial pressures or temperature. Another possibility is that the amplification of the electric current by a multichannel plate, which is necessary in FEM for visualization of the signal, could generate noise as well. In any case, we should expect that the noise of internal origin modelled by the chemical master equation is not the only source of stochasticity in the experiments. The deviations could also be due to the fact that all the processes and interactions at play are not included in the model. It is for example known that additional nonlinearities, which could here arise from additional reactive steps or because of lateral interactions between adsorbates, tend to make stochastic oscillations more robust. Neglecting such contributions can lead to an overestimation of Ω and, thus, to differences in the autocorrelation functions.

These differences are also reflected in the shape of the stochastic craters that can be reconstructed from the time

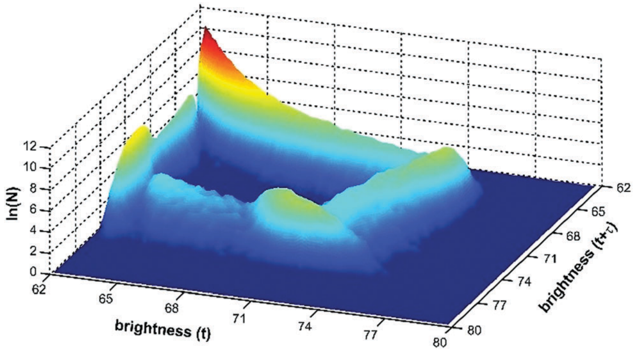

Fig. 10 Stochastic crater obtained by stochastic simulations, with parameter values identical to those of Fig. 8. The histograms were constructed in a way identical to the one presented in Fig. 5.

series of the simulations. An example of such a crater is given in Fig. 10.

To obtain this figure, we followed the same procedure as the one used for experimental time series: we chose a time delay (here 400 ms, like in the experiments), and plotted the probability of occurrence of a $(B(t), B(t + \tau))$ state. Visual comparison between the two probability distributions indicates that the model captures most of the variability of the recorded signal. We note in particular the presence of a global maximum close to the baseline of the signal (appearing in red in Fig. 10) and several local maxima that are located on the ''corners'' of the cycle. However, the slopes of the crater are much steeper in the case of simulation results. The phenomena that we neglected thus not only affect fluctuations along the cycle, which result in a more rapidly decaying autocorrelation function, but also fluctuations transversal to this cycle that lead to more dispersed trajectories, more dispersed amplitudes and, thus, to shallower probability distributions.

VI Conclusions

The role played by fluctuations in reactive systems, including the shape and properties of the stochastic attractors that they define, has been mostly analyzed theoretically. Field Emission Microscopy represents in this context a unique tool to validate these predictions experimentally. The effect of fluctuations on the dynamics of nanoscale systems had been previously assessed with this technique in the case of the bistable $CO + O_2$ reaction on platinum. Fluctuations were shown to induce transitions between states and thus lead to multimodal probability distributions for the signal, in accordance with theoretical predictions.[45,46] In the present work, we analyzed the case of oscillating systems by combining Field Emission Microscopy with time-delay phase space reconstructions and time series analyses. We showed that the oscillations define a deterministic ''backbone'' corresponding to a limit cycle. Due to the small size of the system, fluctuations are present and their combination with the underlying deterministic behavior leads to spontaneous explorations of trajectories away from the cycle. These events lead to the emergence of a stochastic crater when plotting the probability distribution of the system's state in phase space. A simple reaction model was able to reproduce both the existence of the limit cycle and of the associated stochastic crater, which supports the idea that the observed dynamics is of chemical origin.

Further investigations are of course needed to extract more information from the combination of experiments and model. One of the questions that should be assessed in the future is what controls the amplitude of oscillations away from the limit cycle in phase space. The properties of fluctuations along the cycle were already analyzed and were shown to obey a universal scaling law.[14] Such fluctuations induce a phenomenon called phase diffusion resulting in a dispersion of the first return times around their mean. The variance of these first return times is expected to be given by a specific combination of kinetic parameters.[43] However, the properties of fluctuations transversal to such cycle are not known to obey any similar law. *A priori*, one could expect that the intrinsically attracting character of the limit cycle would result in small fluctuations of the amplitude, but this is not always the case. It has been suggested that the divergence of phase space trajectories in the deterministic limit could be a good indicator of the amplitude of such fluctuations.[37] The experimental setup we used here could represent an invaluable tool to verify such proposals on a real-world system.

More importantly, though, we believe that similar studies should be performed to study the elusive case of deterministic chaos, which represents the next step in the complexity of dynamical systems. There has been some controversy in the literature on the observability of deterministic chaos in the presence of noise.[47,48] Some authors advocated that in small systems, the amplitude of fluctuations are amplified due to the intrinsically diverging character of chaotic trajectories in phase space and that, as a consequence, they become of the same order of magnitude as the deterministic trajectories. In this view, the underlying chaos thus cannot be observed. Other authors argued on the other hand that the presence of a strange attractor confers robustness to chaotic dynamics and that a ''blurred'' version of deterministic chaos should be observed. While these questions have been analyzed with the help of simulations,[49,50] nanoscale experiments should help settle this debate. We plan to perform these experiments in a near future.

Conflicts of interest

There are no conflicts to declare.

Acknowledgements

C. B. and V. V. thank the Fonds de la Recherche Scientifique (F.R.S.-FNRS) for financial support (Postdoctoral fellowship and PhD grant, respectively). P. G. acknowledges the financial support of the Fonds de la Recherche Scientifique-FNRS under the Grant PDR T.0094.16 for the project ''SYMSTATPHYS''. The authors gratefully thank the Van-Buuren Foundation for a financial support for the acquisition of equipment and the Wallonia-Brussels Federation (Action de Recherches Concertées no. AUWB 2010-2015/ULB15).

Notes and references

1 T. Visart de Bocarmé, T. Bär and N. Kruse, *Ultramicroscopy*, 2001, **89**, 75.

2 A. Theiss and F. W. Rollgen, *Appl. Surf. Sci.*, 1996, **76/77**, 307.

3 B. Sieben, G. Bozdech, N. Ernst and J. H. Block, *Surf. Sci.*, 1996, **352–354**, 167.

4 C. Barroo, S. V. Lambeets, F. Devred, T. D. Chau, N. Kruse, Y. De Decker and T. Visart de Bocarmé, *New J. Chem.*, 2014, **38**, 2090.

5 R. H. Fowler and L. Nordheim, *Proc. R. Soc. London, Ser. A*, 1928, **119**, 173.

6 R. G. Forbes, *Ultramicroscopy*, 1999, **79**, 11.

7 B. Pennemann, K. Oster and K. Wandelt, *Surf. Sci.*, 1991, **249**, 35.

8 P. T. Dawson and Y. K. Peng, *Surf. Sci.*, 1980, **92**, 1.

9 V. Gorodetskii, J. H. Block and W. Drachsel, *Appl. Surf. Sci.*, 1994, **76/77**, 129.

10 P. D. Cobden, C. A. de Wolf, M. Yu. Smirnov, A. Makeev and B. E. Nieuwenhuys, *J. Mol. Catal. A: Chem.*, 2000, **158**, 115.

11 R. Imbhil, Non-linear Dynamics in Catalytic Reactions, in *Handbook of Surface Science*, ed. E. Hasselbrink and B. I. Lundqvist, Elsevier B.V., Amsterdam, 2008, pp. 342–427.

12 C. Barroo, N. Gilis, S. V. Lambeets, F. Devred and T. Visart de Bocarmé, *Appl. Surf. Sci.*, 2014, **304**, 2.

13 C. Barroo, Y. De Decker, T. Visart de Bocarmé and N. Kruse, *J. Phys. Chem. C*, 2014, **118**, 6839.

14 C. Barroo, Y. De Decker, T. Visart de Bocarmé and P. Gaspard, *J. Phys. Chem. Lett.*, 2015, **6**, 2189.

15 C. Barroo, Y. De Decker, T. Visart de Bocarmé and N. Kruse, *Phys. Rev. Lett.*, 2016, **117**, 144501.

16 A. Gaussmann and N. Kruse, *Catal. Lett.*, 1991, **10**, 305.

17 H. J. Kreuzer and R. L. C. Wang, *Z. Phys. Chem.*, 1997, **202**, 127.

18 J.-S. McEwen, P. Gaspard, T. Visart de Bocarmé and N. Kruse, *J. Phys. Chem. C*, 2009, **113**, 17045.

19 N. Kruse and T. Visart de Bocarmé, Heterogeneous Catalysis and High Electric Fields, in *Handbook of Heterogeneous Catalysis*, ed. G. Ertl, H. Knözinger, F. Schüth and J. Weitkamp, Wiley-VCH Verlag GmbH& Co. KGaA, Weinheim, Germany, 2nd edn, 2008, pp. 870–895.

20 T. T. Tsong, *Surf. Sci.*, 1978, **70**, 211.

21 R. Lewis and R. Gomer, *Surf. Sci.*, 1968, **12**, 157.

22 R. Lewis and R. Gomer, *Surf. Sci.*, 1969, **17**, 333.

23 J. M. Heras and L. Viscido, *Appl. Surf. Sci.*, 1980, **4**, 238.

24 D. Brown, Tracker Video Analysis and Modeling Tool, 2009, http://physlets.org/tracker/.

25 C. Voss and N. Kruse, *Appl. Surf. Sci.*, 1996, **94/95**, 186.

26 C. Voss and N. Kruse, *Ultramicroscopy*, 1998, **73**, 211.

27 C. Barroo, Y. De Decker, L. Jacobs and T. Visart de Bocarmé, *Appl. Surf. Sci.*, 2017, **412**, 564.

28 J.-S. McEwen, P. Gaspard, Y. De Decker, C. Barroo, T. Visart de Bocarmé and N. Kruse, *Langmuir*, 2010, **26**, 16381.

29 C. Barroo, Y. De Decker and T. Visart de Bocarmé, *J. Phys. Chem. C*, 2017, **121**, 17235.

30 J. C. Sprott, *Chaos and Time-Series Analysis*, Oxford University Press, UK, 2003.

31 F. Takens, Detecting strange attractors in fluid turbulence, in *Symposium on dynamical systems and turbulence*, ed. D. A. Rand and L.-S. Young, Springer, Berlin, 1981, pp. 366–381.

32 H. G. Schuster, *Deterministic Chaos: An Introduction*, Wiley-VCH, Germany, 1995.

33 T. Sauer, J. A. Yorke and M. Casdagli, *J. Stat. Phys.*, 1991, **65**, 579.

34 M. B. Kennel, R. Brown and H. D. I. Abarbanel, *Phys. Rev. A: At., Mol., Opt. Phys.*, 1992, **45**, 3403.

35 R. Hegger, H. Kantz and T. Schreiber, *Chaos*, 1999, **9**, 413.

36 Y. De Decker, D. Bullara, C. Barroo and T. Visart de Bocarmé, Nonlinear Dynamics of Reactive Nanosystems: Theory and Experiments, in *Bottom-Up Self-Organization in Supramolecular Soft Matter – Principles and Prototypical Examples of Recent Advances*, ed. S. C. Müller, and J. Parisi, Springer Series in Materials Science 217, Springer International Publishing, Switzerland, 2015, pp. 127–150.

37 D. Gonze, J. Halloy and P. Gaspard, *J. Chem. Phys.*, 2002, **116**, 10997.

38 D. Mei, J. Du and M. Neurock, *Ind. Eng. Chem. Res.*, 2010, **49**, 10364.

39 A. G. Makeev and B. E. Nieuwenhuys, *J. Chem. Phys.*, 1998, **108**, 3740.

40 Q. Ge and M. Neurock, *J. Am. Chem. Soc.*, 2004, **126**, 1551.

41 K. Christmann, *Surf. Sci. Rep.*, 1988, **9**, 1.

42 A. von Oertzen, H. H. Rotermund and S. Nettesheim, *Surf. Sci.*, 1994, **311**, 322.

43 P. Gaspard, *J. Chem. Phys.*, 2002, **117**, 8905.

44 F. G. Cosi and K. Krischer, *Eur. Phys. J.: Spec. Top.*, 2017, **226**, 1197.

45 Yu. Suchorski, J. Beben, E. W. James, J. W. Evans and R. Imbihl, *Phys. Rev. Lett.*, 1999, **82**, 1907.

46 Yu. Suchorski, J. Beben, R. Imbihl, E. W. James, D.-J. Liu and J. W. Evans, *Phys. Rev. B: Condens. Matter Mater. Phys.*, 2001, **63**, 165417.

47 R. F. Fox and J. Keizer, *Phys. Rev. A: At., Mol., Opt. Phys.*, 1991, **43**, 1709.

48 G. Nicolis and V. Balakrishnan, *Phys. Rev. A: At., Mol., Opt. Phys.*, 1992, **46**, 3569.

49 P. Geysermans and G. Nicolis, *J. Chem. Phys.*, 1993, **99**, 8964.

50 V. Voorsluijs and Y. De Decker, *Phys. D*, 2016, **335**, 1.